Chapter 9

Spectral Fitting in HXDS Detector Data Analysis

Richard J. Edgar

9.1 Introduction

This chapter discusses the use of spectral fitting and the `JMKmod` software in the analysis of AXAF calibration data. What is described here is the standard reduction of the data. A somewhat more sophisticated use of `JMKmod` which produces higher fidelity results, but at a significant cost in attention and labor, is described in §9.4.

9.2 Reduction of the Line Measurements

The outputs of the HXDS (HRMA X-ray Detector System; the assemblage of detectors described in the introduction) equipment, for spectral detectors, consists of a pulse-height spectrum for each of the detectors (focal plane plus BNDs), and various derived products based on region-of-interest sums over spectral channels. These are converted into FITS files compatible with the XSPEC X-ray spectral analysis program.

The resulting FITS files are fit to a model which includes the source properties (spectral lines plus a Kramer continuum model, of the form $(E_{max} - E)/E$), the X-ray filter properties, and the detector properties. This model, known as `JMKmod` (Tsiang et al., 1997) is based on the discussion by Jahoda and McCammon (1988) of proportional counter physics, generalized to include solid state detectors. We use a unit diagonal response matrix in XSPEC with this software, allowing us to control all the features of the detector model within our own software, and to adjust detector parameters as well as source parameters to fit the observed spectra. Further details and discussion of the model can be found in Edgar et al. (1997) and Tsiang et al. (1997).

There are in excess of 50 parameters to be set in this model, but the vast majority of them can be set from values obtained from the facility data or experiment design. We then fit the remaining 3 to 6 parameters interactively, once for each type of detector for each source setup. The interesting parameters here are the ones that describe the flux in the spectral line in question (including escape peaks, partial charge-collection "shelf" features in the spectrum, pileup, and other detector effects). Also allowed to float freely in most fits is the relative flux of the continuum and the line.

For a typical fit, all parameters but a few are fixed to theoretical values. The floating parameters typically include either the fano factor or the Polya h parameter (which have nearly identical effects on the line width and shape, and so should never be allowed to vary freely at the same time); the shelf norm (which models partial charge collection); the continuum norm (for EIPS spectra which have a continuum); the overall `JMKmod` norm (*i.e.* the intensity); and escape line energies and norms (if $E > 3$ keV). For SSD spectra, the `broad` (electronic line broadening) can also be allowed to float freely. The energy of the escape peak should be allowed some freedom because of energy nonlinearities such as that shown in Figure 3.6, which shows a discontinuity in the effective ionization energy of the gas across the Ar L-edge.

Some energy/channel nonlinearity is expected in any proportional counter, and it is likely that each detector system has its own small channel offset, but this does not significantly affect our results because the fitting process (and particularly the energy scale determination) is dominated by the main peak. Likewise, slight rate-dependent variations in peak width are automatically accounted for during the fitting process.

As explained in Chapter 5, for SSD spectra above 2 keV, the pileup parameter should be frozen at $1 - 0.6\mu s \times Rate$, if one is using the Gedcke-Hale deadtime estimates from the file headers. Pileup should not be included in the fits if the pulser peak is used to determine the deadtime fraction. Below 2 keV, the incomplete pileup rejection greatly complicates matters.

We show in Table 9.1 a list of the parameters in the `JMKmod` XSPEC model, with their default values, and recommended values for fitting FPC and SSD spectra.

There are numerous effects to be accounted for in such a procedure. Here is a list of those we have done only approximately, with an estimated bias or error at the few percent level for each. They are discussed one by one below.

- Most fits are done by minimizing the χ^2 statistic.
- Backgrounds were modeled rather than subtracted.
- No correction is made for the mesh in the focal plane FPC window.
- Deadtime is estimated by the detector pulse-processing electronics, and we use this estimate.

In cases where there are few counts per channel, the χ^2 statistic, with its built-in assumptions of Gaussian distributed errors, is both inappropriate and biased (Bevington and Robinson, 1992). A more appropriate statistic, the C–statistic, based on maximum likelihood arguments and the Poisson distribution is discussed by Cash (1979), and Nousek and Shue (1989). This statistic is implemented within XSPEC, and we have used it in such cases as wing scans, and some BND fits, which have weak signals. We have verified that in cases with many counts per channel this C–statistic produces comparable results to the conventional χ^2 method.

For the Encircled Energy experiments, the count rates are orders of magnitude above background in every case. Therefore, for these cases, background subtraction or modeling will not be a significant effect. For wing scan spectra, however, this will be important. In those cases, because of poor statistics in the background spectra, we elected to fit a function (often a power law plus broad Gaussian combination) to the background spectrum, and then use this function (with no free parameters) as a component in fitting the X-Ray spectra. This decision was driven in part by a feature of XSPEC which makes use of the C–statistic (see previous paragraph) incompatible with background subtraction. It also eliminates the need to deal with channels which, due to statistical fluctuations, would have a negative count rate if background subtraction were done.

Table 9.1: Parameters for the JMKmod model, with recommended values.

#	Name	Default	FPC	SSD	Remarks
1	fano	0.2	0.2	0.2	Fano factor; line width
2	polyah	1.2	1.2	ignored	Polya H param; line width for FPC
3	E_offset	0.0	0.0	0.0	zero−point offset in E scale (keV)
4	i_pot	2.8e−2	2.8e−2	3.0e−3	energy per ion pair, keV
5	gain	4.0	.5−−4.0	0.6	gain in channels/ion pair
6	ch_off	0.0	0.0	0.0	zero−point offset in channel scale
7	broad	0.0	0.0	10.0	electronic Gaussian broadening (chans)
8	d_gain	0.0	0.0	0.0	width of top hat gain distribution
9	nchan	512.	512.	4096.	number of channels
10	sestype	1.	1.	1.	1=FPC 2=SSD 3=FPC w/distrib gain
11	contin	1.	1.	1.	1=yes 0=no continuum
12	econt	10.	10.	10.	high energy cutoff of continuum (keV)
13	contnorm	1.	.1	.1	norm of continuum, rel to line
14	E_max	10.	10.	10.	max energy for contin; set = param 12
15	E_min	0.01	0.01	0.01	min energy for contin (keV)
16	E_char	2.	2.	2.	characteristic energy for Gaussian continuum
17	E_width	0.1	0.1	0.1	width of Gaussian continuum (keV)
18	nInt	512.	512.	512.	number of points in contin integral
19	temper	15.	15.	ignored	FPC temp (C) for QE only
20	pressure	400.	400.	ignored	FPC pressure (torr) for QE only
21	argrat	0.9	0.9	ignored	proportion of Argon; rest is CH4
22	shelfsw	0.	0.	0.	1=yes; 0=no low energy shelf
23	t1norm	0.	0.	0.	falling tail norm
24	t1par	0.999	0.999	0.999	falling tail scale length
25	t2norm	0.	0.	0.	rising tail norm
26	t2par	1.001	1.001	1.001	rising tail scale length
27	shelfnm	0.	0.	0.	flat shelf norm
28	pulser	0	0	0	1=yes 0=no pulser peak fit
29	pulsepos	100.	100.	100.	position of Gaussian pulser (chans)
30	pulsesig	1.	1.	1.	sigma of Gaussian pulser peak (chans)
31	pulsenrm	1.	1.	1.	norm of Gaussian pulser peak
32	numcomp	2.	2.	2.	Number of lines *DO NOT CHANGE*
33	numfil	6.	6.	6.	Number of "filters" *DO NOT CHANGE*
34	pileup	0	0	0	1=yes 0=no pileup
35	pilepar	1.	0.999	0.999	pileup parameter
36	bfield	1.45e4	1.45e4	1.45e4	B(gauss) for synchrotron model
37	current	1.	1.	1.	beam current (amps) for synch mod
38	incline	0.	0.	0.	inclination (deg) for synch mod
39	abswitch	0.	0.	0.	1=yes 0=no absolute norm for synch mod
40	phi	135.40	135.40	135.40	azimuth angle (deg) for A_eff filt
41	theta	40.20	40.20	40.20	off−axis angle (deg) for A_eff
42	shell	12.	12.	12.	mirror combo for A_eff
43	E_line1	1.49	1.49	1.49	Energy of line 1 (keV)

Table 9.1: (continued)

#	Name	Default	FPC	SSD	Remarks
44	E_line2	1.56	1.56	1.56	Energy of line 2 (keV)
45	E_norm1	1.	1.	1.	norm of line 1 (set to 1)
46	E_norm2	1.	1.	1.	norm of line 2 rel to line 1
47	src1	35.	35.	35.	src/filter 1 (kramer continuum)
48	src2	6.	6.	6.	src/filter 2 (carbon XSS filter)
49	src3	2.	2.	2.	src/filter 3 (Al in window)
50	src4	19.	19.	19.	src/filter 4 (polyimide in window)
51	src5	38.	38.	37.	src/filter 5 (FPC or SSD body QE)
52	src6	45.	45.	45.	src/filter 6 (unused)
53	srcthk1	0.	0.	0.	thickness of flt 1 (unused)
54	srcthk2	2.5e−4	2.5e−4	2.5e−4	thickness of flt 2 (cm)
55	srcthk3	2.e−6	2.e−6	2.e−6	thickness of flt 3 (cm)
56	srcthk4	1.065e−4	1.065e−4	1.065e−4	thickness of flt 4 (cm)
57	srcthk5	5.36	5.686	0.5	thickness of flt 5 (cm)
58	srcthk6	0.	0.	0.	thickness of flt 6 (cm)
59	norm	1.	?	?	overall norm (counts/sec)

The FPC detectors have a mesh of 100 μm diameter wires on 2 mm centers to support their plastic windows against the pressure differential. For the BND detectors, which are uniformly illuminated, we have reduced the working area by the fraction of the geometrical area obscured by this mesh. For the focal plane detector, a focused, on-axis image will fit within a single mesh cell, and an effort was made to place the focused image at the center of such a mesh cell. Mesh obscuration is extremely small in on-axis cases without gratings. Proper accounting for this effect is done by a ray trace simulation of the mirrors and FPCs. This effect is discussed in further detail in Chapter 6.

Note that the fitted counting rates are in *counts* s^{-1}. To get photons per second, the detector quantum efficiency must be divided into the counting rate. In many cases of phase 1 measurements, we can use relative quantum efficiencies, which in some cases are better known than the absolute ones.

Detector dead time is estimated by the detector operating software using a Gedcke-Hale technique, and we adopt this estimate (which is recorded in each raw spectral file header). An electronic pulser input was included in nearly all spectra, and a comparison of pulses injected to pulses detected will allow a more accurate dead time correction. While work remains to be done on the accuracy of this estimate, The Gedke-Hale deadtime matches that determined from the pulser peak to much better than 1% for FPC spectra. For SSD measurements, the pulser peak is used to determine the deadtime. This is further complicated by incomplete pileup rejection below 2 keV (see Chapter 4).

9.3 A Sample Fit: Ti K–α

In this section we discuss a sample JMKmod fit. The data in question are an fpc_5 spectrum of the EIPS, with a Ti anode and the source high voltage set to about 15 kV, with a Ti filter which is about 2 mean free paths thick at Ti K–α. This results in a spectrum which contains the Ti K–α and K–β lines, and a bremsstrahlung continuum. Much of the continuum just hardward of the

lines is absorbed by the filter.

We fit a spectral model using the `JMKmod` software, with parameters as shown in Figure 9.1. The model consists of four δ-function lines: Ti K–α (4.51 keV), Ti K–β (4.93 keV), and the Ar K–α escape lines of these two, at the above energies minus 2.9577 keV. There is also a Kramer continuum of the form $(E_{max} - E)/E$, with E_{max} in keV set numerically equal to the source high voltage in kV.

We allowed the following parameters to float freely: the detector gain, the continuum norm (ratio of continuum counts to the K–α line counts), and the overall norm (total counting rate).

Note that the residual, while nearly flat, has a systematic wiggle in it which indicates that our model is not an entirely adequate description of the actual pulse height spectrum. We adjust the gain, line shape parameters, etc. to minimize this wiggle, and in cases where it cannot be eliminated, we make the (eyeball) integral of the residual near zero, so that the error in the line countrate is a small fraction of the amplitude of the wiggle, which in turn is a small fraction of the amplitude of the line. In this case, we obtain $\chi^2_\nu = 0.9888$, though in many cases the reduced χ^2 value exceeds unity.

We plot the results in Figure 9.2.

9.4 A Higher Fidelity Method for Analysis of FPC Line Data

The data were processed in much the same way as the generic XRCF FPC data, as described in §9.2. In order to improve the fidelity of the analysis, however, certain systematic effects need to be accounted for, which necessitates additional care in some aspects of the data reduction.

One such effect is to include the (rough) shape of the HRMA effective area curve in the analysis. This changes not the counting rate at the line, but rather the shape of the continuum. Fitting the continuum well allows one to confidently separate continuum photons that fall in the region of the line from line photons, and to quote a counting rate due to line photons only, despite the poor intrinsic resolution of the FPC detectors.

Many of the tests covered here are encircled energy (EE) tests, which have many iterations using different sizes of pinhole apertures on the focal plane detector. After verifying that the counting rates measured by the BND-H detectors are time-independent, the data from all these iterations (or those where a given detector was functioning, if it went offline for some of them) were co-added, to improve the signal to noise ratio for further analysis.

Unlike the `fpc_5` and focal plane FPC detectors, the BND-H detectors have a substantial amount of open area, approximately 3.6 × 9.9 cm. The response of these single-wire flow proportional counters has been found to be quite uniform across the wire (in the Y direction at XRCF), but the gain is significantly higher near the ends of the detectors. Prior to the calibration, the blocking plate apertures were reworked, giving a somewhat smaller open area and masking the ends of the counters where the gain was largest. However, there is still enough variation of gain along the wire that it must be taken into account in order to obtain acceptable fits to the spectra.

The `fpc_hn` detector could be used either open, or with a 35 mm circular aperture. When used with the 35 mm aperture, the gain nonuniformity effect is negligible.

As shown in §3.4, the gain distribution for the various counters is nearly the same, and they are quite flat for the central ∼ 6 cm of each counter. Then, to good approximation, the gain increases nearly linearly to the ends of the active part of the counter. Thus the gain distribution can be approximated as a delta function plus a top-hat function extending from the center-section gain value to some larger value. Fortunately, both delta function and top-hat function (*i.e.* constant between two given values of x, and zero elsewhere) gain distributions are available within the


```
XSPEC> show all
15:53:03 16-Sep-98
Auto-saving is done after every command.
Fit statistic in use is Chi-Squared
Minimization technique is Lev-Marq
  Convergence criterion =    1.0000000000000D-02
Querying enabled
Prefit-renorming enabled
Solar abundance table is angr

  Information for file   1
   belonging to plot group   1, data group   1
  telescope = HXDS , instrument = fpc_5 , channel type = PHA
    Current data file: acq1114040310.fits
    No current background
    No current correction
    Response (RMF) file    : /home/edgar/diag512.rmf
    Auxiliary (ARF) file   : none
  Weighting method is standard
    Noticed channels    9 to   469
    File integration time    11.14
      and effective area     1.000
    File observed count rate    2384.    +/- 14.650     cts/s
    Model predicted rate :    2347.

  mo = jmkmod4[1]
  ------------------------------------------------------------------------------
  mo = jmkmod4[1]
  Model Fit Model Component  Parameter  Unit     Value
  par  par comp
    1    1   1  jmkmod4   fano      null      0.1432       frozen
    2    2   1  jmkmod4   polyah    null      1.215        frozen
    3    3   1  jmkmod4   E_offset  keV       0.           frozen
    4    4   1  jmkmod4   i_pot     null      2.8000E-02 frozen
    5    5   1  jmkmod4   gain      chan/pai  1.197      +/- 0.6200E-03
    6    6   1  jmkmod4   ch_off    chan      0.           frozen
    7    7   1  jmkmod4   broad     null      0.           frozen
    8    8   1  jmkmod4   d_gain    null      0.           frozen
    9    9   1  jmkmod4   nchan     null      512.0        frozen
   10   10   1  jmkmod4   sestype   null      1.000        frozen
   11   11   1  jmkmod4   contin    null      1.000        frozen
   12   12   1  jmkmod4   ecout     keV       15.30        frozen
   13   13   1  jmkmod4   contnorm  null      6.2624E-02 +/- 0.6074E-02
   14   12   1  jmkmod4   E_max     keV       15.30      = par  12
   15   14   1  jmkmod4   E_min     null      1.0000E-02 = par  12
   16   15   1  jmkmod4   E_char    null      2.000        frozen
   17   16   1  jmkmod4   E_width   null      0.1000       frozen
   18   17   1  jmkmod4   temp      C         512.0        frozen
   19   18   1  jmkmod4   pressure  torr      15.00        frozen
   20   19   1  jmkmod4   pressure  torr      400.0        frozen
   21   20   1  jmkmod4   argrat    null      0.9000       frozen
   22   21   1  jmkmod4   shelfsw   null      1.000        frozen
   23   22   1  jmkmod4   t1norm    null      0.           frozen
   24   23   1  jmkmod4   t1par     null      0.9990       frozen
   25   24   1  jmkmod4   t2norm    null      0.           frozen
   26   25   1  jmkmod4   t2par     null      1.001        frozen
   27   26   1  jmkmod4   shelfnm   null      1.0000E-02 frozen
   28   27   1  jmkmod4   pulser    null      0.           frozen
   29   28   1  jmkmod4   pulsepos null      100.0        frozen
   30   29   1  jmkmod4   pulsesig null      1.000        frozen
   31   30   1  jmkmod4   pulsenrm null      1.000        frozen
   32   31   1  jmkmod4   numcomp   null      4.000        frozen
   33   32   1  jmkmod4   numfil    null      6.000        frozen
   34   33   1  jmkmod4   pileup    null      0.           frozen
   35   34   1  jmkmod4   pilepar   null      1.000        frozen
   36   35   1  jmkmod4   bfield    gauss     1.4500E-04 frozen
   37   36   1  jmkmod4   current   mA        1.000        frozen
   38   37   1  jmkmod4   incline   rad       0.           frozen
   39   38   1  jmkmod4   abswitch  null      0.           frozen
   40   39   1  jmkmod4   phi       deg       135.4        frozen
   41   40   1  jmkmod4   theta     arcmin    40.20        frozen
   42   41   1  jmkmod4   optconst  null      0.           frozen
   43   42   1  jmkmod4   E_line1   keV       4.510        frozen
   44   43   1  jmkmod4   E_line2   null      1.520        frozen
   45   44   1  jmkmod4   E_line3   null      4.932        frozen
   46   45   1  jmkmod4   E_line4   null      1.934        frozen
   47   46   1  jmkmod4   E_norm1   null      1.000        frozen
   48   47   1  jmkmod4   E_norm2   null      6.7203E-02 frozen
   49   48   1  jmkmod4   E_norm3   null      0.           frozen
   50   49   1  jmkmod4   E_norm4   null      1.2443E-02 frozen
   51   50   1  jmkmod4   src1      null      35.00        frozen
   52   51   1  jmkmod4   src2      null      14.00        frozen
   53   52   1  jmkmod4   src3      null      2.000        frozen
   54   53   1  jmkmod4   src4      null      19.00        frozen
   55   54   1  jmkmod4   src5      null      38.00        frozen
   56   55   1  jmkmod4   src6      null      45.00        frozen
   57   56   1  jmkmod4   srcnk1    cm        0.           frozen
   58   57   1  jmkmod4   srcnk2    null      4.3850E-03 frozen
   59   58   1  jmkmod4   srcnk3    null      2.0000E-06 frozen
   60   59   1  jmkmod4   srcnk4    null      1.0650E-04 frozen
   61   60   1  jmkmod4   srcnk5    null      5.360        frozen
   62   61   1  jmkmod4   srcnk6    null      0.           frozen
   63   62   1  jmkmod4   norm                2065.      +/-  15.07
  ------------------------------------------------------------------------------
  Chi-Squared =          460.6877     using   461 PHA bins.
  Reduced Chi-squared =  1.005868     for   458 degrees of freedom
  Null hypothesis probability = 0.456
  XSPEC> ipl
  XSPEC> ipl
  XSPEC> quit
  Do you really want to exit (y)y
  XSPEC: quit
```

Figure 9.1: Sample `JMKmod` log file, obtained with the `show all` command in `XSPEC`

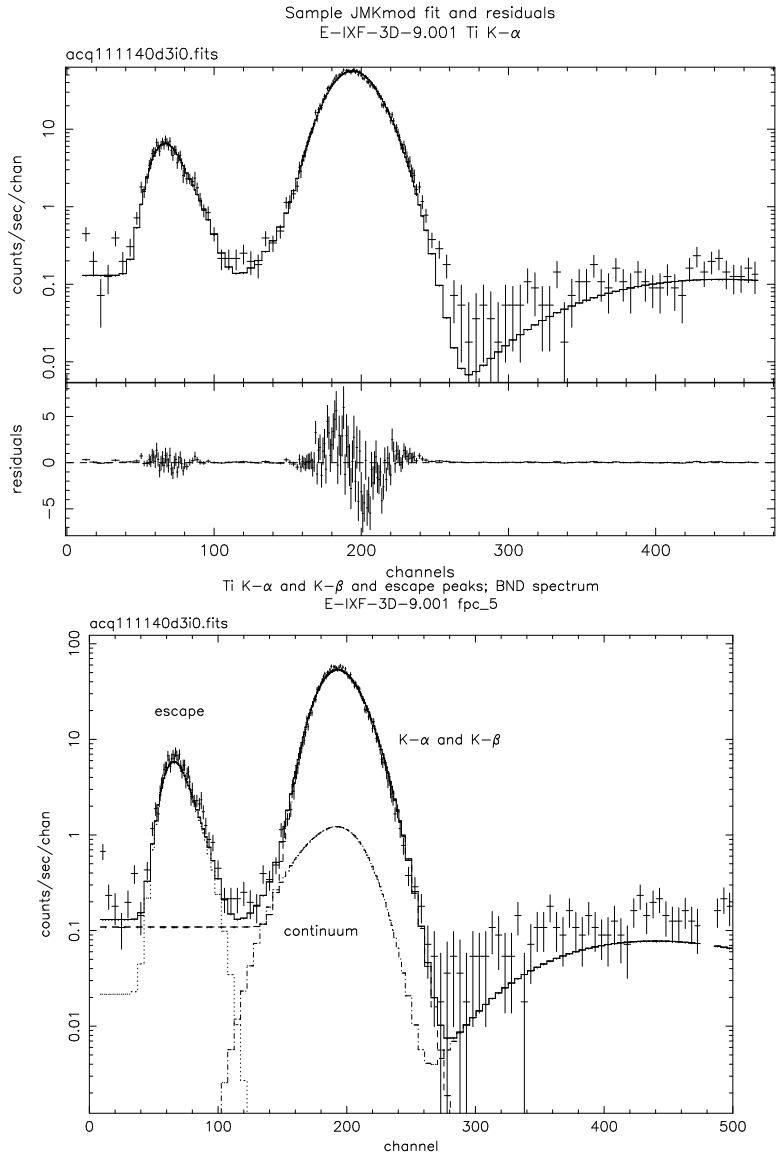

Figure 9.2: Sample `JMKmod` spectral fit to Ti K–α spectrum. Upper panel: data (+ signs), model (solid curve) and residuals in the same units as the upper plot. Lower panel: data and three model components. This shows that the continuum contributes $\sim 1\%$ to the counting rate in the main bump.

`JMKmod` version 7.0 software as it was released in December 1996.

We thus use not a single `JMKmod` component as a model, but two `JMKmod` components, with nearly all their parameters linked together (*i.e.* constrained to have the same value for both models). The exceptions are the `gain` (central section gain for model 1 and the middle of the top-hat function for model 2), `dgain` (the half-width of the top-hat function for model 2), and the normalizations of the two models. This permits excellent fits with small residuals and reduced χ^2 values. The line count rate is then the sum of the line norms for constituent lines of the complex (for example, K–α and K–β and their escape peaks), times the sum of the overall norms for the two `JMKmod` model components.

The recommended parameters for this type of model are these:

- $gain_1$ is the gain of the delta function center-section model.
- $gain_2 = gain_1 \times 1.05$. This is the central gain of the top-hat function gain distribution.
- $dgain_2 = gain_1 \times 0.1$. This is the full width of the top-hat function gain distribution.
- $norm_2 = norm_1 \times 0.7241$. This represents the relative wire length involved in each of the two gain distributions (delta function and top-hat).
- $sestype_1 = 1$ (delta-function gain distribution), and $sestype_2 = 3$ (top-hat gain distribution function).

9.5 Analysis of BESSY FPC Monochromator data

During the periods December 4–7, 1997 and January 20–23, 1998, two of the FPC detectors were calibrated at BESSY. During this time, a number of runs were done at various energies with the SX-700 monochromator, in the energy range from 0.08 to 1.7 keV. This monochromator beamline is well calibrated, and ring currents and x-ray intensities in photons per second per unit ring current are known to 0.5% at most energies.

We have analyzed these data using the `JMKmod` fit procedure outlined in §9.2, using as a model a delta-function line convolved with the `JMKmod` FPC response. In addition, it was necessary over the energy range from the carbon edge at 0.284 keV to about 0.300 keV to introduce a continuum to the fit, peaked sharply about 1 keV, due to a low level of leakage of photons near 1 keV through the monochromator. These are normally down 5 or more orders of magnitude relative to the main line, but in this particular energy range, the quantum efficiency of the detector at the main line is $\sim 10^{-5}$ or less, while around 1 keV the QE is ~ 0.7. In practice, we found it sufficient to model this extra component with another spectral line with energy near 1 keV and floating, and floating normalization relative to the main line.

The counter high voltage was set to correspond to a central energy for each scan, and then the monochromator was scanned through a number of energy settings, with the FPC at the same setting. We adjusted the gain parameter of the detector model in accordance with the standard FPC tuning practice, namely $gain \propto E_{target}^{-1/2}$ with a gain of 1 channel per ion pair (one ion pair is fixed at 28 eV in these fits) at about 4.5 keV. This was then allowed to float over a narrow range to compensate for possible temperature effects on the gain. The counting rate and these parameters are then fit.

We also allowed a few of the line shape parameters (Fano factor, and shelf norm) to vary. The Polya h parameter is set to its default value of 1.2. In practice the Fano factor and h have nearly indistinguishable effects on the line width and shape, and so only one of these two parameters was

allowed to vary. The resulting fitted Fano factor may not be physically reasonable, but the fits to the data closely match the observed line shape nonetheless.

Also freely varying was the pileup parameter, which is the fraction of the counts not involved in x-ray/x-ray pileup collisions. The line count rate is then divided by this parameter to reconstruct the total detected counting rate, including pileup effects. The pulser peak and higher pulse height channels were ignored, as were the first 8 channels, below the lower level discriminator. This analysis of the data produces results in general within 1% of the counting rates obtained by PTB from region of interest analysis of the pulse height spectra.

We present in Figure 9.3 and Figure 9.4 plots of the line shape parameters as functions of energy. Note the jump in the shelf norm occurs at the Ar L edge at 248 eV. This happens since the gas becomes much more opaque just hardward of this edge, and so the x-rays are converted to charge clouds closer to the window, resulting in more charge loss to the window than for softer photons.

Note also that the shelf is not well constrained by the data at very low energies (below about 0.2 keV) since the peak is at such low pulse height that most of the shelf is moved below the lower level discriminator.

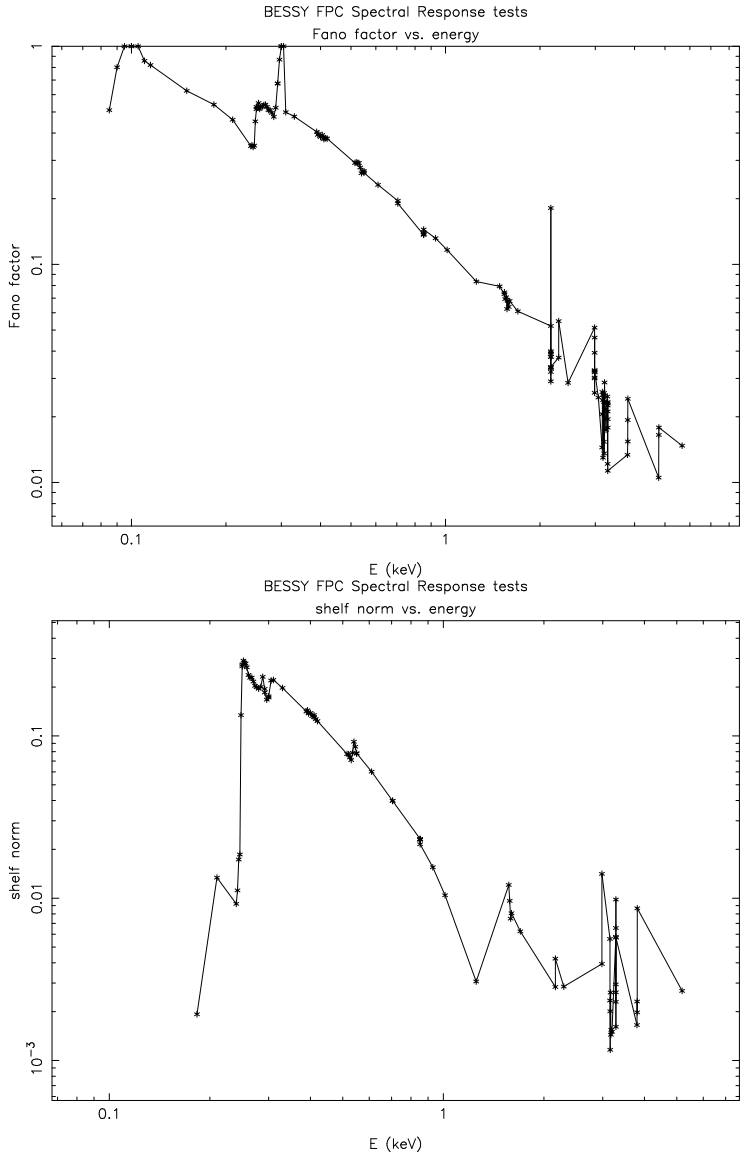

Figure 9.3: Line shape parameters for the fpc_x2 as functions of energy. Top: Fano factor, and Bottom: Shelf norm

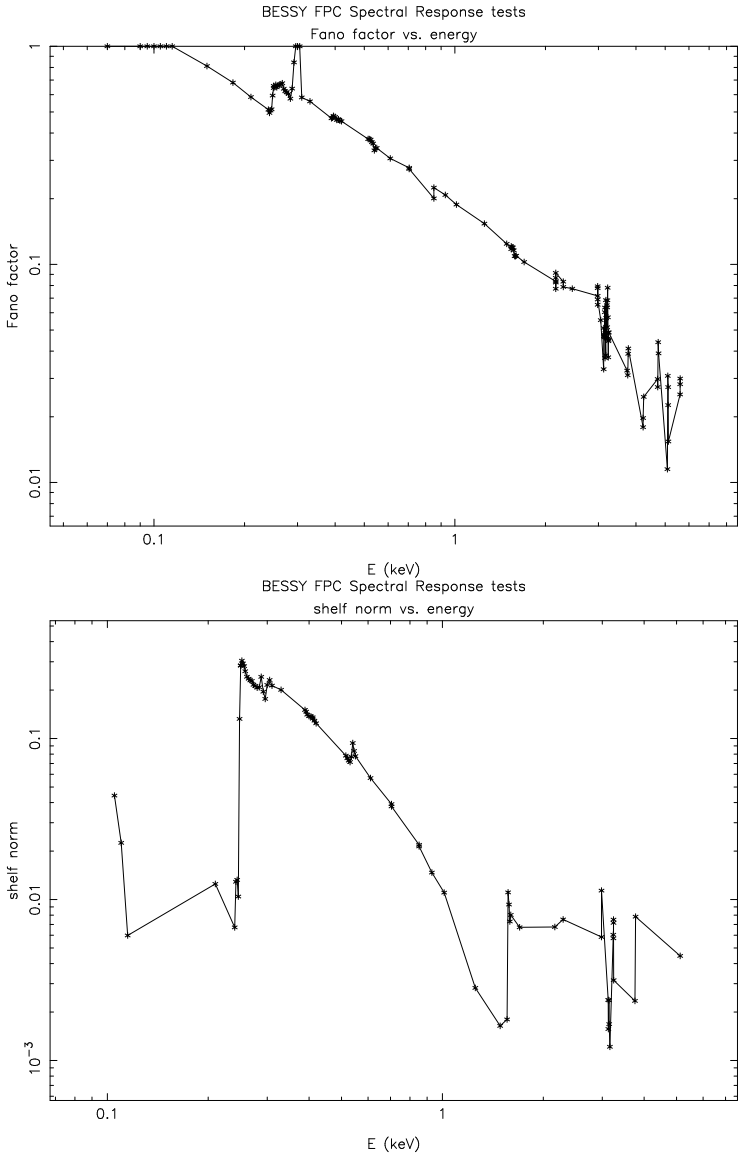

Figure 9.4: Line shape parameters for the fpc_hn as functions of energy. Top: Fano factor, and Bottom: Shelf norm